DOI: 10.1002/cssc.201000379

Electrocatalytic Carbon Dioxide Activation: The Rate-Determining Step of Pyridinium-Catalyzed CO_2 Reduction

Amanda J. Morris, Robert T. McGibbon, and Andrew B. Bocarsly*[a]

The reactivity of reduced pyridinium with CO_2 was investigated as a function of catalyst concentration, temperature, and pressure at platinum electrodes. Concentration experiments show that the catalytic current measured by cyclic voltammetry increases linearly with pyridinium and CO_2 concentrations; this indicates that the rate-determining step is first order in both. The formation of a carbamate intermediate is supported by the data presented. Increased electron density at the pyridyl nitrogen upon reduction, as calculated by DFT, favors a Lewis acid/base interaction between the nitrogen and the CO_2. The rate of the known side reaction, pyridinium coupling to form hydrogen, does not vary over the temperature range investigated and had a rate constant of $2.5\,\text{M}^{-1}\,\text{s}^{-1}$. CO_2 reduction followed Arrhenius behavior and the activation energy determined by electrochemical simulation was $(69 \pm 10)\,\text{kJ mol}^{-1}$.

Introduction

Carbon dioxide, a potent greenhouse gas, is thought to be a main contributor to global climate change.[1] The concentration of atmospheric CO_2 is increasing; this is due in part to anthropogenic sources, including the burning of fossil fuels.[2] Therefore, the mitigation of industrial carbon dioxide emissions has become a priority, and much research is being dedicated to its efficient capture and sequestration. Present discussion appears to favor storage in underground geologic structures as an option for carbon mitigation. However, another approach that may be advantageous is the chemical conversion of carbon dioxide to a value-added product. One potential approach that has garnered recent industrial interest is the formation of a chemical fuel, for example, an alcohol, starting with a CO_2 feedstock.[3–4]

Bocarsly et al. reported the low overpotential conversion of CO_2 to methanol at hydrogenated palladium electrodes using pyridinium as a homogeneous catalyst in the 1990s.[5] That work was recently expanded to include photoelectrochemical CO_2 reduction at illuminated *p*-GaP electrodes.[6] The Faradaic efficiency for conversion of CO_2 to methanol neared 100% when the *p*-GaP electrode was held at an underpotential of 220 mV (based on the standard reduction potential for CO_2 conversion to methanol by six electrons and protons, $E^\circ = -0.52$ V vs. SCE at pH 5.3). To date, the pyridinium-catalyzed reduction of CO_2 is the most efficient reported method for photoelectrochemical methanol formation.

Recent mechanistic investigations have suggested key intermediates involving the formation of pyridyl N–C bonds in the overall reaction scheme.[7] These species are responsible for the reduction of CO_2 through a series of one-electron transfer steps. This is in direct contrast to previously reported CO_2 reduction catalysts that are believed to operate by multielectron charge-transfer (MET) pathways. Multiple-electron-transfer catalysis can offer an immense advantage over single-electron-transfer pathways. For example, the reduction of CO_2 by one electron to form the $CO_2^{\bullet-}$ requires -2.14 V versus SCE. If instead CO_2 accepts six reducing equivalents and protons to form methanol this can occur at the more moderate potential of -0.62 V versus SCE (pH 7). Pyridinium-catalyzed reduction of CO_2 is the first case, to the best of our knowledge, in which six sequential one-electron proton-coupled transfers provide the low-energy route for catalysis. This is significant because many could have historically overlooked one-electron-transfer catalysts for traditional multiple-electron-transfer catalysis, that is, proton reduction, water oxidation, and carbon dioxide reduction.

Herein, we report the dependence of the aforementioned reactivity on catalyst concentration, CO_2 pressure, and temperature. The measurement of the reaction rate as a function of these physical properties reveals further mechanistic insight. Of particular importance is the determination of the overall rate-determining step. Although the ultimate aim of this research is the efficient light-driven reduction of CO_2 at a semiconductor electrode, the complex electrochemical behavior of the reduction at such an interface precludes direct mechanistic studies. To overcome this complication, CO_2 reactivity was investigated at platinum electrodes. The applicability of the mechanistic information gathered in this study to reactivity at illuminated *p*-GaP electrodes is discussed. In addition to fundamental implications, this study examines the electroreduction of CO_2 under a set of conditions that may be of importance for the development of an industrial CO_2 conversion process based on this technology.

[a] *Dr. A. J. Morris, R. T. McGibbon, Prof. A. B. Bocarsly*
Department of Chemistry
Princeton University
Princeton, NJ 08536 (USA)
Fax:(+1) 609-258-2902
E-mail: bocarsly@princeton.edu

Results and Discussion

In the presence of CO_2, the pH of an aqueous electrolyte solution (0.5 M KCl) containing 10 mM pyridine is dependent on the established carbonic acid/pyridine buffer and is sensitive to both temperature and dissolved CO_2 concentration. To determine the concentration of dissolved species, the pH was measured as a function of temperature and pressure. The pH of the solution remained constant at 5.3 over the temperature range investigated (0–45 °C). However, the pH decreased with increased CO_2 pressure (i.e., [CO_2 (aq)]): from 5.3 at 1 atm to 4.6 at 5 atm. The dependence of relevant CO_2 equilibria as a function of temperature and pressure have been previously determined and were utilized to calculate the concentration of species present under reaction conditions.[10] For example, the concentration of dissolved CO_2 determined by using the appropriate Henry's Law constant (e.g., 0.03 mol L^{-1} atm^{-1} for 25 °C) at 0.5 M ionic strength was 0.033 M. It is important to note that at the pH values investigated the concentration of HCO_3^- would be at most 10% of the overall dissolved carbon species ($pK_a = 6.3$).[10] Thus, within the accuracy of the data provided herein, one can assume that all of the reactive carbon is available as CO_2 (aq). It is also important to note that CO_2 (aq) is the catalytically reducible species and bicarbonate is inactive to reduction by pyridinium.[5]

At the measured pH values, a portion of the aqueous pyridine is protonated to yield electroactive pyridinium cations that are reversibly reduced at −0.58 V versus SCE at pH 5.3 (Scheme 1). In contrast, pyridine is reduced by two electrons at approximately −2.76 V versus Ag/AgCl, as measured in DMF.[11] Thus, protonation of the pyridyl nitrogen reduces the reduction potential by over two volts. Since pyridine is neutral and pyridinium is charged, one would expect a 59 mV shift in reduction potential per pH unit. Therefore, charge-only arguments cannot fully explain the observed shift in half-wave potential. The protonation of the pyridyl nitrogen, additionally, has an immense effect on the π* level (LUMO) of the molecule and DFT calculations indicate that there is a 1.4 eV shift in the LUMO level upon protonation. The additional potential shift can be explained by the difference in reorganization energy required for the formation of a neutral one-electron-reduced molecule capable of hydrogen bonding (pyridinium) in aqueous solution versus a radical anion (pyridine) in nonaqueous electrolyte.

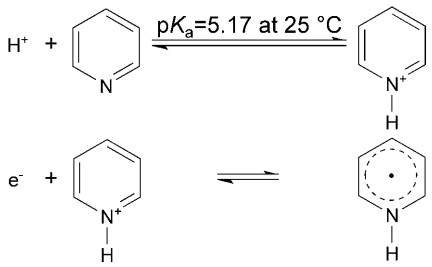

Scheme 1. Protonation and reduction of aqueous pyridine to yield the one electron reduced pyridyl radical.

The reduction of pyridinium was studied under an argon atmosphere in a pH-adjusted solution (Scheme 1 b). The pH was adjusted such that it matched the natural buffer pH measured for a similar sample under a CO_2 atmosphere. The cyclic voltammograms showed a nonreversible wave with a peak–peak separation greater than 60 mV (Figure 1). Nicholson and Shain diagnostics indicate that the scan-rate-dependent peak-to-peak separation is due to an underlying electrocatalytic mechanism.[12] It has been previously reported that the reduction of pyridinium in proton-containing solution is coupled to the electrocatalytic formation of hydrogen by two pyridinium radicals (Scheme 2).[7,11] We have previously applied this mechanism to explain the behavior observed.[7]

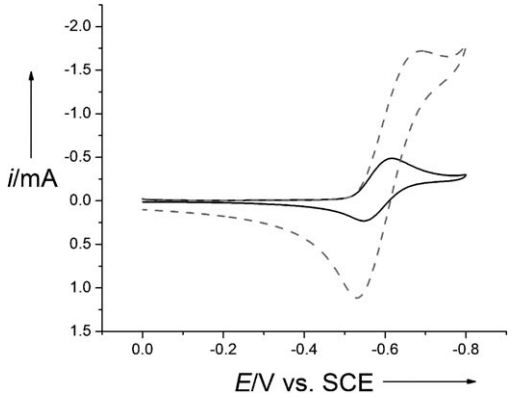

Figure 1. Cyclic voltammograms of 10 mM pyridine in a aqueous solution of 0.5 M KCl at pH 5.3 under an Ar atmosphere (——) and under a CO_2 atmosphere, 0.033 M [CO_2 (aq)] (-----). Both scans were recorded at 5 mV s^{-1}.

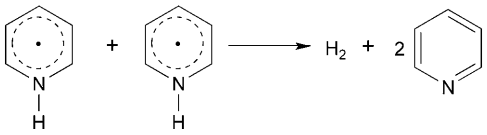

Scheme 2. Electrocatalytic formation of hydrogen from two pyridinium radicals.

There was no discernable temperature dependence to the anodic and cathodic peak currents observed in the cyclic voltammograms of aqueous pyridinium reduction under an Argon atmosphere and were, within error, the same over the temperature range investigated (0–45 °C). There was a slight decrease in peak-to-peak separation, which is attributed to an increase in kinetics of either the aforementioned chemical step (k_{H_2}; Scheme 2) or the heterogeneous charge-transfer rate constant (k_{et}; Scheme 1 b). Electrochemical modeling of the cyclic voltammograms show that pyridinium radical coupling is temperature independent over the temperature range studied; consistent with the reported lack of cathodic current change. The rate constant for proton reduction (k_{H_2}) was calculated to

be (2.3 ± 0.5) M^{-1} s^{-1}. The rate constant for heterogeneous electron transfer to pyridinium (k_{et}) determined in these simulations increased slightly as a function of temperature and was found to be 1.15×10^{-3} (2.5), 4.22×10^{-3} (10), 5.67×10^{-3} (25), 6.61×10^{-3} (35), and 6.86×10^{-3} (45 °C).

Pyridinium catalytically reduced CO_2, as evidenced by the enhancement of the cathodic current in a cyclic voltammogram of 10 mM pyridine in an aqueous solution under a CO_2 atmosphere compared with a voltammogram collected for a pH-adjusted, Ar-saturated solution (Figure 1). The current was found to increase linearly with increased pyridinium concentration over the range 1 to 6 mM and saturate at higher concentrations (Figure 2 inset). Thus, the rate-limiting step of the reaction is first order in pyridinium over this concentration range. At higher concentrations (8–32 mM), the current change was equal to that observed under an argon atmosphere. Therefore, above 8 mM pyridinium the catalytic current is assigned to a combination of CO_2 reduction and proton reduction, the latter process dominating as the concentration of pyridinium is increased. The saturation behavior observed for pyridinium reactivity with CO_2 is suggestive of a surface reaction under these conditions. However, saturation of the concentration curve may also be due to the fact that CO_2 has become the limiting reagent as the concentration of pyridinium increases.

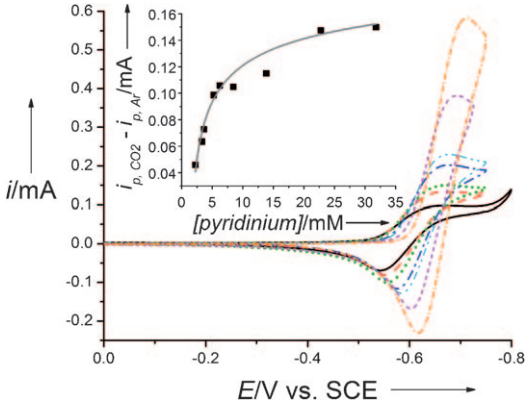

Figure 2. Cyclic voltammograms collected at 5 mV s^{-1} for pyridinium concentrations of 2.24 (black), 3.32 (red), 3.65 (green), 5.24 (blue), 6.25 (cyan), 13.84 (magenta), and 22.75 mM (orange) in a 0.5 M aqueous solution of KCl under a CO_2 atmosphere (0.033 M [CO_2 (aq)]). The inset shows the dependence of the differential cathodic peak current (measured as the difference between the cathodic peak current of the cyclic voltammogram of pyridinium, pH-adjusted and under an Argon atmosphere, to the peak current for pyridinium reduction in the presence of CO_2). The concentration of pyridinium was corrected for the solution pH.

The nature of the surface reaction is specifically relevant because Pt electrodes are expected to behave differently from the *p*-GaP electrodes previously investigated. While the initial reduction of pyridinium at both platinum and *p*-GaP electrodes was reported to be a solution process,[7] the electrode surface may provide a mechanism for the destabilization of the reduced pyridyl N–H bond that facilitates CO_2 binding to the nitrogen site. Pyridinium has the majority of its electron density at the pyridyl nitrogen (Figure 3). Upon reduction this electron density increases, which makes the nitrogen a stronger Lewis base and thus, it binds the proton more tightly. Increased Lewis basicity has long been identified as necessary for CO_2 binding.[13] It is likely that high electron density in this position promotes the stability of a pyridine radical–CO_2 bond. However, the initially reduced species has a tightly bound proton that diminishes the electron density on the nitrogen and theoretically blocks the putative CO_2 binding site. The surface may be key in the dissociation of the reduced pyridyl N–H bond. This destabilization process is hypothesized to be the same at platinum and *p*-GaP and it is only the fate of the proton that differs at the electrode surfaces. Platinum surface metal sites are known to stabilize surface hydrides that then react to form hydrogen.[14] This would result in lower Faradaic yields for methanol at Pt electrodes because some current is lost to proton reduction, which is consistent with experimental observations at electrodes with a low overpotential for hydrogen production.[5] The surface of *p*-GaP, however, consists of an oxide layer, which can be protonated, but due to the high overpotential of proton reduction at *p*-GaP will not form hydrogen readily. This is also consistent with previous results of extremely high methanol Faradaic yield at *p*-GaP photoelectrodes because surface protonation does not lead to competitive hydrogen evolution.[6] Further investigation is currently underway to elucidate the identity of the surface-dependent step(s) and the importance of chemisorption processes in the overall mechanism.

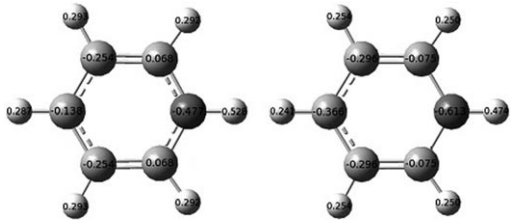

Figure 3. Partial charges for pyridinium (left) and the pyridinium radical (right) were determined by natural bond orbital (NBO) analysis with the Gaussian 03 program.[18] The calculations show that the majority of the electron density lies on the pyridyl nitrogen (dark grey) in both pyridinium and the pyridinium radical. They also show that the electron density on the nitrogen increases upon reduction thus decreasing the N–H bond length.

The dependence of the electrochemical behavior on the concentration of CO_2 was measured by increasing the pressure of CO_2 from 1 to 6 atm (Figure 4). At the scan rate shown, 5 mV s^{-1}, it appears that over this pressure range there is a transition from mass transport limitation at low pressure to a kinetic limitation at high pressure, as evidenced by a loss in a distinguishable reduction peak in the cyclic voltammogram. The maximum peak current increased by a factor of 3.5 when the pressure was increased to 6 atm. The dependence of peak current on pressure and, therefore, CO_2 concentration was linear over the pressure range investigated with no indication that linearity changes beyond that. Thus, the reaction is overall second order, within the concentration ranges investigated, and is first order in both pyridinium and carbon dioxide.

Based on the above findings and previously reported electrochemical data,[6–7] the formation of a pyridinium radical–CO_2

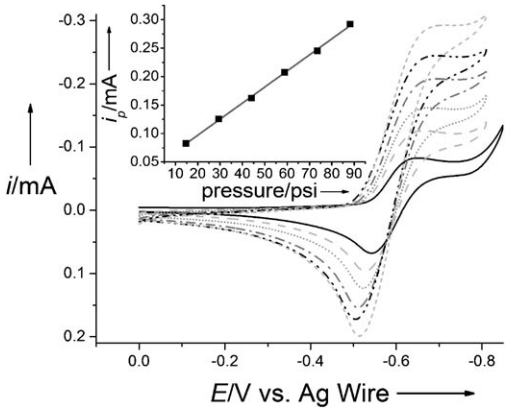

Figure 4. Cyclic voltammograms collected at 5 mV s^{-1} for 10 mM pyridine in a 0.5 M aqueous solution of KCl under 14.1 (solid), 28.2 (dash), 42.3 (dot), 56.4 (dash dot), 70.5 (dash dot dot), and 84.6 psi (short dash) of CO_2. The inset shows the dependence of the maximum cathodic peak current on the concentration of CO_2. The concentration of CO_2 was determined by using the appropriate Henry's law constant (0.03 mol L^{-1} atm^{-1}).

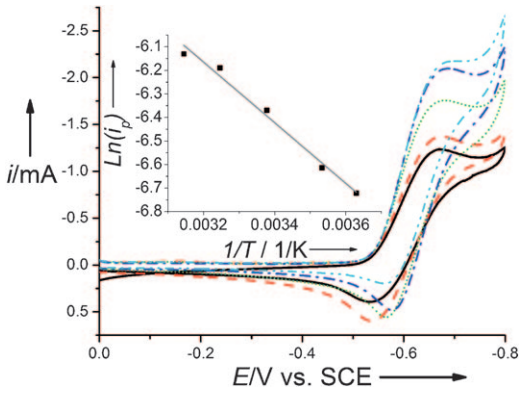

Figure 5. Cyclic voltammograms collected at 5 mV s^{-1} for 10 mM pyridine in a 0.5 M aqueous solution of KCl under CO_2 atmosphere at 2.5 (black), 10 (red), 23 (green), 35 (blue), and 45 °C (cyan). The inset shows a logarithmic inverse temperature dependence of the maximum cathodic peak current. The peak current shown in the inset was corrected for dissolved CO_2 concentration.

complex, a one-electron-reduced carbamate-like species, is proposed as the rate-determining mechanistic step (Scheme 3).[1,15] In support of this conclusion, a distinct UV/Vis spectrum attributed to a carbamate species was collected during the electrochemical reduction of CO_2 in the presence of *n*-propyl-4,4′-bipydinium.[16]

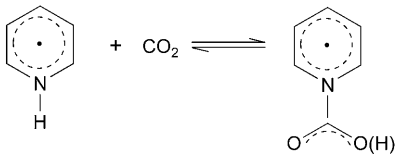

Scheme 3. Formation of a the pyridinium radical–CO_2 complex.

The temperature dependence of pyridinium-catalyzed CO_2 reduction was investigated for the temperature range (0–45 °C). The cathodic current, which followed an Arrhenius-like dependence, was observed to increase with increased temperature (Figure 5). Additionally, the peak-to-peak separation decreased upon an increase in temperature; this was indicative of faster kinetics or decreased resistance. Nicholson and Shain diagnostics indicate that at all temperatures the same mechanism is followed.

The electrochemical data measured for temperature-dependent CO_2 reactivity were digitally simulated by using the reactions shown in Schemes 1–5, and the results are provided in Figure 6. Schemes 4 and 5 account for the electrochemical behavior of the carbamate and the regeneration of the initial cat-

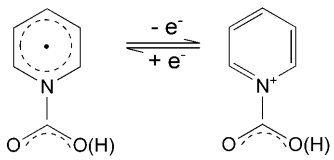

Scheme 4. Electrochemical behavior of the carbamate.

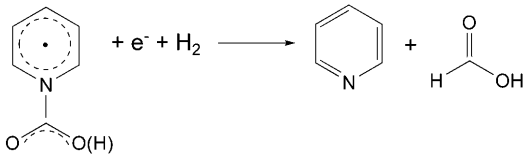

Scheme 5. Reduction of the carbamate intermediate to yield formic acid and regenerate pyridine.

alytic species. Scheme 2 accounted for the anticipated side reaction; pyridinium radical coupling to generate hydrogen. The values for k_{et} and k_{H_2} determined by the aforementioned independent modeling for pH-controlled CO_2 free cells were held constant in the simulated electrochemical behavior of CO_2-containing cells, thus the number of independent variables was reduced. The reduction potential for the carbamate species was found to be approximately 100 mV more negative than that of pyridinium at −0.66 V versus SCE.

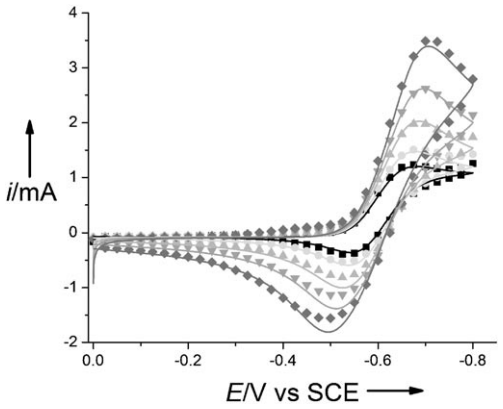

Figure 6. Cyclic voltammograms collected at 2.5 °C for 10 mM pyridine in a 0.5 M aqueous solution of KCl under CO_2. The scan rates shown are 5 (■), 10 (●), 25 (▲), 50 (▼), and 100 mV s^{-1} (◆). The corresponding lines are the simulated cyclic voltammograms obtained by fitting the curves to the mechanism discussed.

Based on this model, the computed rate constants for the formation of the carbamate-like species were found to follow an Arrhenius relationship that yielded an activation barrier of (69 ± 10) kJ mol^{-1} (Figure 7). This activation barrier is within the

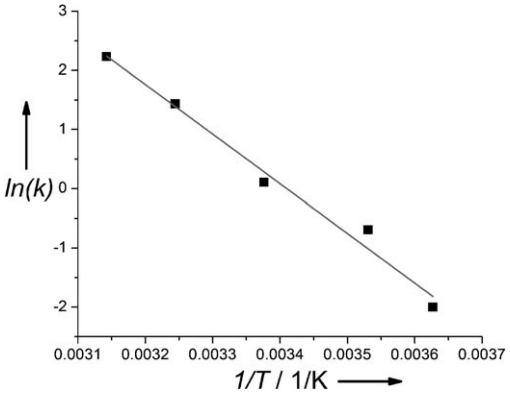

Figure 7. Arrhenius plot for the dependence of the rate constant for carbamate formation on temperature. The rate constants were obtained by simulation of the experimental cyclic voltammograms for the reactions shown in Schemes 1–5. The slope of the line indicates an activation barrier of (69 ± 10) kJ mol^{-1}.

range of other reported activation barriers for catalyzed reactions.[17] Based on the resultant pre-exponential factor, a decrease in this activation energy by a factor of 3 would increase the rate constant to $\approx 10^8$ M^{-1} s^{-1}, which is near the diffusion limit. This might be achieved by manipulating the nitrogen basicity of the pyridyl moiety.

Conclusion

The pyridinium-catalyzed reduction of CO_2 was investigated as a function of catalyst concentration, CO_2 concentration, and temperature. At platinum electrodes, the reaction was found to occur through a surface-active, site-dependent, rate-determining step that is first order in both CO_2 and pyridinium. The formation of an intermediate carbamate is strongly supported by the data obtained. An Arrhenius analysis of the results indicates that the activation barrier for pyridinium-catalyzed CO_2 reduction is (69 ± 10) kJ mol^{-1}. The data provided herein suggest that two factors may increase reaction kinetics: 1) the Lewis basicity of the pyridyl nitrogen and 2) the ability of the electrode surface to stabilize carbon-based free radicals. To study the effect of increased Lewis basicity on the reaction kinetics, substituted pyridines with electron-donating groups may be utilized. However, there is a delicate balance between kinetics and thermodynamics underlying the observed reactivity. While increased electron-donating ability of the pyridyl nitrogen is predicted to increase reaction rate, this would also stabilize the carbamate species. For product formation the carbamate must dissociate and, therefore, a highly stable carbamate is not desired. Studies are presently underway to explore the reaction rate and product formation in regards to these parameters.

Experimental Section

Materials

Potassium chloride (>99%, EMD), pyridine (>99.9%, Aldrich), sulfuric acid (EMD), hydrochloric acid (EMD), nitric acid (EMD), and carbon dioxide (99.8%, Airgas) were used as received. Deionized water was used to prepare the aqueous electrolyte solutions.

Electrochemical measurements

Cyclic voltammetry: Polarization curves were collected on a CH Instruments 760D potentiostat. A standard three-electrode arrangement was used with a known area Pt foil (1.93 cm^2, Aldrich) or wire (0.005 cm^2, diameter: 1 mm, length: 6.65 mm, Aldrich) working electrode, Pt mesh (Aldrich) counter electrode, and reference electrode (SCE, Accumet or Ag wire, Aldrich) immersed in an aqueous solution of pyridine (10 mM unless otherwise indicated) and KCl (0.5 M). Scan rates ranged from 5 to 200 mV s^{-1}. Prior to experiment and in between each change in temperature or pressure the electrodes were immersed in concentrated sulfuric acid or nitric acid, rinsed with deionized water, and flamed by using a natural gas torch. Before cyclic voltammetric scans were collected, the solution was purged for 10–45 min with Ar or CO_2. To preserve the desired gaseous atmosphere during the experiment, a constant flow of gas was maintained in the cell head space. In between each pressure and temperature change the electrolyte solution was replaced with fresh bulk solution. All potentials are referenced to the SCE electrode unless otherwise indicated.

Temperature and pressure conditions

Temperature: The temperature was controlled by using an Isotemp stir plate fitted with a thermocouple temperature probe. A secondary temperature measurement was made with a thermometer. The experiments were conducted at $\approx$2 (ice bath), $\approx$10 (water bath), $\approx$20 (RT), $\approx$30 (oil bath), and $\approx$45 °C (oil bath). The pH of the electrolyte solution under CO_2 was measured to be 5.3 over this temperature range after temperature compensation was employed. Under Ar the pH was adjusted to 5.3 with 0.1 M H_2SO_4 at all temperatures investigated. Water evaporation rates precluded measurement at temperatures above 50 °C, at which temperatures electrolyte concentration changes due to solvent evaporation could not be accurately reproduced.

Pressure: Pressure experiments were conducted in a custom glass cell (Figure 8). The glass cell, rated to operate up to 250 psi, utilized curved interior surfaces for improved high-pressure stability. The pressures applied were kept at half the rated level and a blast shield was used at all times. Approximately 35 mL of the 0.5 M aqueous solution of KCl containing 10 mM pyridine added to the cell. The pressure was applied 45 min before measurement to allow the concentration of dissolved CO_2 to equalize. Pressures investigated were 14.1, 28.2, 42.3, 56.4, 70.5, and 84.6 psi. The pH of the solution decreased with pressure and was 5.3, 5.0, 4.9, 4.8, 4.8, 4.7, for the respective pressures listed above.

Calculations

DFT: Estimates of the LUMO energies of the pyridine and pyridinium redox mediator system were made by using the Gaussian 03 program.[18] The geometries of pyridine and pyridinium were optimized at the spin-unrestricted B3LYP/631++G(d,p) level of theory in H_2O by using the polarizable continuum model (PCM) solvation

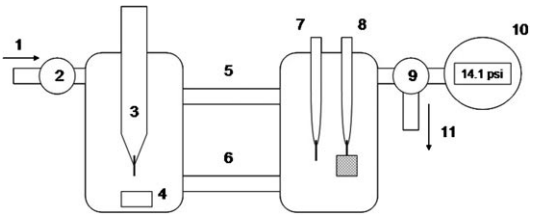

Figure 8. Glass vessel used for the electrochemical reduction of CO_2 under high pressure: 1) gas inlet, 2) inlet valve, 3) Ag wire reference electrode 4) stirrer bar, 5) connection tube, pressure equalizer, 6) solution bridge, 7) Pt wire electrode, 8) Pt mesh electrode, 9) three way valve, 10) pressure gauge, and 11) gas vent.

model. The absence of imaginary vibrational frequencies characterized the geometries as minima. Partial charges were determined by NBO analysis.

Electrochemical simulations: Simulations of cyclic voltammograms were generated with the use of DigiElch 4.0 software. The diffusion coefficients for all species were estimated as 1×10^{-5} cm s^{-1}. All experimentally fixed parameters (i.e., scan rate, electrode area, etc.) were set as fixed parameters in the simulation runs. The competitive rate for hydrogen production was determined by electrochemical modeling of cyclic voltammograms collected during independent pH-controlled experiments under Ar and utilized the reactions shown in Schemes 1 and 2 as fitting parameters. The concentration of [H^+] was set to the bulk concentration measured experimentally as 4.5×10^{-6} M. The K_a of pyridine as a function of temperature was calculated by using the van 't Hoff equation based on the reported pK_a at 25 °C (5.17[8]) and ΔH° of 4.8 kcal mol^{-1},[9] to yield values of 3.5×10^{-6} (2.5), 4.40×10^{-6} (10), 6.33×10^{-6} (25), 8.80×10^{-6} (35), 1.13×10^{-5} (45 °C). The rate of electron transfer (k_{et}) to pyridinium was also determined in these independent simulations. The reduction potential for pyridinium, as determined by the modeling software, was −0.58 V versus SCE. As discussed in the text, to simulate cyclic voltammograms collected in the presence of CO_2, the reactions shown in Schemes 1–5 were entered as fitting parameters. The H^+ concentration, E^o, K_a, k_{H_2}, and k_{et} values previously determined by the independent modeling discussed above were imported. The concentration of CO_2 was determined from the appropriate Henry's Law Constants and was 0.062 (2.5), 0.048 (10), 0.032 (25), 0.023 (35), 0.019 M (45 °C). The experimental simulations determined the E^o, α, and k values for the remaining electron-transfer and chemical steps.

Acknowledgements

This work was funded by the Division of Chemical Sciences, Geosciences, and Biosciences, Office of Basic Energy Sciences of the U.S. Department of Energy through Grant DE-SC0002133.

Keywords: carbon dioxide · catalysis · electrochemistry · energy conversion · pyridinium

[1] M. M. Halmann, M. Steinberg, *Greenhouse Gas Carbon Dioxide Mitigation*, Lewis, New York, **1999**.
[2] *Climate Change 2001: Synthesis Report. A Contribution of Working Groups I, II, and III to the Third Assessment Report of the Integovernmental Panel on Climate Change* (Ed.: R. T. Watson), Cambridge University Press, New York, **2001**.
[3] E. B. Cole, A. B. Bocarsly, *Carbon Dioxide as Chemical Feedstock* (Ed.: M. Aresta), Wiley-VCH, Weinheim, **2010**.
[4] A. J. Morris, G. J. Meyer, E. Fujita, *Acc. Chem. Res.* **2009**, *42*, 1983.
[5] G. Seshadri, C. Lin, A. B. Bocarsly, *J. Electroanal. Chem.* **1994**, *372*, 145.
[6] E. E. Barton, D. M. Rampulla, A. B. Bocarsly, *J. Am. Chem. Soc.* **2008**, *130*, 6342.
[7] E. Barton Cole, P. S. Lakkaraju, D. M. Rampulla, A. J. Morris, E. Abelev, A. B. Bocarsly, *J. Am. Chem. Soc.* **2010**, *132*, 11539.
[8] H. C. Brown, X. R. Mihm, *J. Am. Chem. Soc.* **1955**, *77*, 1723.
[9] C. L. Liotta, E. M. Perdue, H. P. Hopkins, *J. Am. Chem. Soc.* **1974**, *96*, 7308.
[10] J. N. Butler, *Carbon Dioxide Equilibria and Their Applications*, Lewis, Michigan, **1991**.
[11] H. Baumgartel, K.- J. Retzlav, *Encyclopedia of Electrochemistry of the Elements, Vol. XV* (Ed.: A. J. Bard), Marcel Dekker, New York, **1973**, p. 194.
[12] R. S. Nicholson, I. Shain, *Anal. Chem.* **1964**, *36*, 706.
[13] E. Fujita, C. Creutz, N. Sutin, D. J. Szalda, *J. Am. Chem. Soc.* **1991**, *113*, 343.
[14] J. O. M. Bockris, A. K. N. Reddy, *Modern Electrochemistry*, Plenum, New York, **1970**.
[15] N. McCann, D. Phan, X. Wang, W. Conway, R. Burns.; M. Attalla, G. Puxty, M. Maeder, *J. Phys. Chem. A* **2009**, *113*, 5022; M. Attalla, G. Puxty, M. Maeder, *J. Phys. Chem. A* **2009**, *113*, 5022.
[16] H. Ishida, T. Ohba, T. Yamaguchi, K. Ohkubo, *Chem. Lett.* **1994**, *23*, 905.
[17] G. C. Bond, *Heterogeneous Catalysis*, Clarendon, Oxford, **1986**.
[18] Gaussian 03, Revision c.02, M. J. Frisch, G. W. Trucks, H. B. Schlegel, G. E. Scuseria, M. A. Robb, J. R. Cheeseman, J. A. Montgomery, Jr., T. Vreven, K. N. Kudin, J. C. Burant, J. M. Millam, S. S. Iyengar, J. Tomasi, V. Barone, B. Mennucci, M. Cossi, G. Scalmani, N. Rega, G. A. Petersson, H. Nakatsuji, M. Hada, M. Ehara, K. Toyota, R. Fukuda, J. Hasegawa, M. Ishida, T. Nakajima, Y. Honda, O. Kitao, H. Nakai, M. Klene, X. Li, J. E. Knox, H. P. Hratchian, J. B. Cross, V. Bakken, C. Adamo, J. Jaramillo, R. Gomperts, R. E. Stratmann, O. Yazyev, A. J. Austin, R. Cammi, C. Pomelli, J. W. Ochterski, P. Y. Ayala, K. Morokuma, G. A. Voth, P. Salvador, J. J. Dannenberg, V. G. Zakrzewski, S. Dapprich, A. D. Daniels, M. C. Strain, O. Farkas, D. K. Malick, A. D. Rabuck, K. Raghavachari, J. B. Foresman, J. V. Ortiz, Q. Cui, A. G. Baboul, S. Clifford, J. Cioslowski, B. B. Stefanov, G. Liu, A. Liashenko, P. Piskorz, I. Komaromi, R. L. Martin, D. J. Fox, T. Keith, M. A. Al-Laham, C. Y. Peng, A. Nanayakkara, M. Challacombe, P. M. W. Gill, B. Johnson, W. Chen, M. W. Wong, C. Gonzalez, J. A. Pople, Gaussian, Inc., Wallingford CT, **2004**.

Received: November 5, 2010

